Stark effect in triatomic hydrogen Rydberg states

Christian Bordas* and Hanspeter Helm
Molecular Physics Laboratory, SRI International, 333 Ravenswood Avenue, Menlo Park, California 94025
(Received 25 June 1991)

The influence of an external electric field on the Rydberg states of triatomic hydrogen has been studied from the viewpoint of the structure of the spectra and the dynamics of the excited states. Rydberg states with principal quantum numbers ranging from 30 to 125 were observed, and low-field as well as very-strong-field regimes investigated. A perturbative treatment taking into account the coupling between the core rotation and the Rydberg-electron motion was developed. The good knowledge of the low-l Rydberg series in H_3 (ns, np, nd, and nf) allowed us to achieve this treatment without adjustable parameters. The agreement between calculation and experimental results is excellent and reveals features resulting from predissociation of selected members of the Stark manifold. Accidental predissociations due to vibrationally excited interlopers are clearly distinguished from the systematic predissociation induced by the mixing with the ns Rydberg series. This is a complete perturbative treatment of the Stark effect in molecular Rydberg states.

PACS number(s): 33.80.Rv, 33.55.Be

I. INTRODUCTION

The influence of an external electric field on atomic and molecular spectra is one of the oldest problems of spectroscopy. The Stark effect was discovered in 1913, and the theory of its effect in atomic hydrogen was the first application of perturbation theory in quantum mechanics [1]. Nowadays, the hydrogenic Stark effect is a textbook application of quantum mechanics [2,3].

Despite this early interest in the Stark effect and its historical importance, the Stark effect in excited states of nonhydrogenic systems has long been rather poorly known owing to several experimental and theoretical difficulties. With the advent of tunable dye lasers in the 1970's, most of the experimental problems have been overcome and interest in this phenomenon has been renewed: Recent investigations of the Stark effect of Rydberg states in alkali metal [4–9] and, more recently, in alkaline-earth atoms [10,11] and rare-gas atoms [12–16] show that it is still a dynamic field of investigation.

The theoretical difficulties are more serious and are still a subject of development. The large number of theoretical papers concerned with the Stark effect during the past 15 years is a good indication of these difficulties. Most of the theoretical works are concerned with the purely hydrogenic Stark effect. For example, Silverstone has derived perturbative calculations to an arbitrarily high order [17], and Luc-Koenig and Bachelier [18] and Damburg and Kolosov [19] have developed exact quantum calculations, including ionization effects. Nonhydrogenic systems have been studied by perturbative methods [4,14] and, more recently, by a multichannel quantum-defect theory (MQDT) [20–25] that takes advantage of the hydrogenic properties of the Stark Hamiltonian.

The Schrödinger equation of a hydrogen atom in an electric field is separable in parabolic coordinates [2,3]. Although the equation is not analytically solvable, this particular symmetry is fundamental and leads to the existence of exact quantum numbers. However, exact quantum numbers cannot be defined in any nonhydrogenic system where the parabolic symmetry is broken.

An essential problem related to the treatment of the Stark effect is the following: As soon as an external electric field is present, the potential experienced by the outer electron decreases monotonically in the direction opposite to the field, with the consequence that the electronic motion is (strictly speaking) unbounded and leads to resonances of finite width. This causes divergence of the perturbation series. At sufficiently high fields, quasidiscrete structures disappear. Another problem, although less fundamental, is also very serious in the practical analysis of the Stark effect in nonhydrogenic systems: Calculation of the Stark spectra of any species requires, in principle, knowing all of the zero-field states (that is, all the quantum defects), and in a multielectron system, the electric field induces additional couplings between the Rydberg electron and ionic core that must be taken into account. This last factor is generally dramatic in a molecule where the electric field couples all the l and J values, and the perturbation basis becomes prohibitively large. Combined with the usually fragmented information about the various l series, this aspect often precludes a standard perturbative treatment of the molecular Stark effect. Extension of the MQDT [20–25] to include an electric field could, in principle, avoid or at least reduce these obstacles. However, the MQDT treatment of the Stark effect in simple molecules such as diatomic hydrogen [23] or sodium dimer [25] is presently not complete.

These difficulties together with the relative lack of information about molecular Rydberg series as compared with atoms explain why, almost 80 years after the discovery of the Stark effect, the molecular Stark effect is still an open field of investigation. The effects of an external electric field on highly excited molecules have mainly been studied from the point of view of the dynamics in-

volved. Glab and Hessler, for example, have studied field-induced predissociation [26] in H_2, and electric-field ionization has been analyzed in various molecules such as H_2 [26], Na_2 [27], and Li_2 [28]. Electric-field ionization of H_3 is planned to be discussed in a forthcoming paper [29] on the basis of the model described here. However, these studies did not include analysis of the Stark effect. With the exception of the fragmentary results of Seaver *et al.* [30] on NO and Cooper *et al.* [31] on H_2, the only comparable study performed so far on a molecular system was done on Na_2. Partly resolved Stark spectra of the Rydberg series of the sodium dimer have been recorded [32], and these spectra in the weak-field regime have been analyzed in the framework of MQDT [25]. However, the limited knowledge of the quantum defects in Na_2 allowed only a qualitative approach. In contrast, the limited character of electron-core interactions and detailed knowledge of the various quantum defects in triatomic hydrogen make a complete analysis of that molecule more easily feasible.

The Stark effect in the molecular Rydberg series is of general interest, but three specific aspects of its relationship to the Rydberg states of H_3 motivated this study.

First of all, if one wishes to investigate in detail the influence of an electric field on molecular Rydberg states, H_3 is one of the best choices because it provides a unique opportunity for studying a complex molecular system having many quasihydrogenic properties. An extensive description of the general aspects of the Rydberg states of H_3 (symmetries, classification, calculated energies, and oscillator strengths) is given by King and Morokuma [33]. Because of the small size of the ionic core (the equilibrium internuclear distance in the ground state of H_3^+ is 0.86 Å; in comparison, that of H_2^+ is 1.06 Å), penetration effects are weak and most of the quantum defects are small. For the same reasons, the core energies are extremely high even in the lowest rotational level and rarely is more than one core level involved in our spectra ($N^+=1$). The gap [34] between the first two ortho levels of H_3^+ ($N^+=1$ and 3, $K^+=0$) is 429.9 cm^{-1}, far larger than the separation between the Rydberg states considered here (less than 8 cm^{-1} for $n=30$). Thus electron-core interactions and couplings are weak compared to those of any other molecule. From this point of view, a comparison of the Rydberg spectra of diatomic [35] and triatomic hydrogen reveals stronger rovibrational interactions in H_2.

A second interesting aspect of the Stark effect in a molecule is the possible onset of chaos. A fairly large amount of work is now being performed with Rydberg atoms in electric or magnetic fields, or both, to understand the correspondence between the quantum mechanics of the atom (and a hypothetical quantum chaos) and classical chaotic motion. In molecular Rydberg states, classical chaos may occur even without an external field, as described by Lombardi *et al.* [36]. However, the presence of an external perturbation which introduces a coupling of adjustable strength may considerably enrich this possibility. Before studying "quantum chaos" in a molecule-plus-field system, it is crucial to understand qualitatively the Stark effect in a relatively simple system such as H_3.

Finally, this work is the logical continuation of the general study of the Rydberg series of H_3 started a few years ago by Helm and co-workers. The *np* [37], *nd* [38,39], and *nf* [40] series of H_3 as well as other aspects [41] of the dynamics of this fundamental molecule have been investigated recently in our group or elsewhere [42,43]. The *nd* series, the most extensively studied, has been investigated by one-photon excitation from the metastable $\tilde{B}(2p)^2A_2''$ state in a fast neutral beam. While the energy levels of this series are well described by the simple Rydberg formula, the line intensities are strongly perturbed. Very intriguing window features appear in the photoionization spectrum. In a previous paper [44], the presence of interlopers belonging to vibrationally excited series that are coupled to the dissociative ground state has been invoked to explain this phenomenon. To understand the extreme sensitivity of some of these windows to the external field and the appearance of similar features in the *np* Rydberg series, we have systematically studied the evolution of the Rydberg spectrum as a function of the field strength. We can observe not only the Stark effect itself, but also the evolution of the interactions between the Rydberg states and dissociative interloper states.

In the next section, we present a short overview of the Stark effect in atomic hydrogen. From this simple model, we discuss the order of magnitude of the field effects and the difference between hydrogenic and nonhydrogenic Stark effects.

After a short description of our experimental techniques, we present low-resolution Stark spectra for principal quantum numbers ranging from 30 to about 125 and higher-resolution spectra for $n=34$. In both cases, there are strong differences according to whether the experiments were performed with the laser polarization parallel or perpendicular to the Stark field. These results are first analyzed with the help of the simple hydrogenic model. We then introduce a perturbative theory that takes into account all the interactions, but has the restriction that the H_3^+ core itself is not affected by the field. The agreement between experimental and theoretical spectra is satisfactory in view of the complexity of the molecular system and the fact that the model includes no adjustable parameters. Differences between predicted and observed spectra appear when the electric field induces decay channels that remove Rydberg population prior to their detection.

We finally compare the respective abilities of the perturbative model used in the present case and a more sophisticated multichannel quantum-defect theory presented elsewhere [20–25].

II. SUMMARY OF THE HYDROGENIC STARK EFFECT

The hydrogenic Stark effect and separation of the Schrödinger equation in parabolic coordinates is presented in quantum-mechanics textbooks [2,3] and described in detail in many papers [17–21]. This summary merely

reviews the basic results of the theory to indicate the order of magnitude of the field effects and to outline qualitatively the Stark effect in a nonhydrogenic system.

The nonrelativistic Coulomb-plus-Stark Hamiltonian of a hydrogen atom in an electric field F directed along the z axis is

$$H=-\frac{\hbar^2}{2m}\Delta-\frac{e^2}{r}+eFz \ . \tag{1}$$

The total wave function ψ, the solution of the Schrödinger equation for a particular energy E,

$$H\Psi=E\Psi \ , \tag{2}$$

is exactly separable in parabolic coordinates,

$$\xi=r+z, \quad \eta=r-z, \quad \phi=\arctan(y/x) \ , \tag{3}$$

and may be written as

$$\Psi(\xi,\eta,\phi)=\Xi(n_1,\xi)\Upsilon(n_2,\eta)e^{im\phi} \ , \tag{4}$$

where the parabolic quantum numbers $\{n_1,n_2,m\}$, which are related to the principal quantum number n via the relation

$$n_1+n_2+|m|+1=n \ , \tag{5}$$

replace the spherical quantum numbers $\{n,l,m\}$.

Note that in a nonhydrogenic atom, m is still a good quantum number, while n_1 and n_2 are not defined because the separability in parabolic coordinates does not hold. The principal quantum number n is strictly conserved in the nonrelativistic approximation in hydrogen, but it is a good quantum number in the other systems at only low-field strength.

At the first order of the perturbation theory, the energy of a (n_1,n_2,m) level is [2,3]

$$E(n_1,n_2,m)=-\frac{1}{2n^2}+\frac{3}{2}nF(n_1-n_2)$$

(in atomic units [45]) , (6a)

$$E(n_1,n_2,m)=-\frac{\mathcal{R}}{n^2}+\alpha nF(n_1-n_2)$$

(in customary units) , (6b)

where $\mathcal{R}$ is the Rydberg constant for hydrogen, F is the electric field, and the constant α is $0.640\times10^{-4}\ \mathrm{V}^{-1}$.

At large values of η, the effective potential along the η axis is proportional to $-F\eta$ and no real bound states exist. However, below the classical saddle-point energy $(-2\sqrt{F})$, the states are quasidiscrete, while above this energy the states are field ionized and broaden rapidly as the field increases. In fact, in atomic hydrogen, the ionization threshold corresponds to the classical saddle-point energy only for $n_1=0$ and $m=1$. The actual ionization threshold is strongly dependent on the value of the parabolic quantum number via the separation constant β [21] [$\beta\approx(2n_1+m+1)/2n$ at low field] and is approximately equal to $[(1-\beta)F]^{1/2}$ (see Ref. [29]). There are two direct consequences of Eq. (6) taken together with relation (5).

(i) For a given m value, a given n state is split into $(n-|m|-1)$ sublevels (the sublevels being separated by $3nF$), which constitute a manifold having a width $\simeq 3n^2F$.

(ii) As the electric field increases, the successive manifolds overlap. This happens when the width of the n manifold $(3n^2F)$ equals the energy separation between two Rydberg states (n^{-3}). The field strength F_c corresponding to this effect is called the Inglis-Teller limit. In atomic units [45],

$$F_c=\frac{1}{3n^5} \ . \tag{7}$$

For a given value of the principal quantum number, the Inglis-Teller limit defined by Eq. (7) determines the relative strength of the applied electric field.

In a nonhydrogenic system, a Rydberg electron with low angular momentum penetrates the core and the departure of the short-range interaction from a pure Coulomb potential is the source of the major part of the quantum defects and the reason that the symmetry of the effective potential is broken. The consequence is a coupling between the different n manifolds. As long as the n and $n\pm1$ manifolds do not overlap, the intramanifold coupling (n mixing) is negligible and n is almost a good quantum number. However, as soon as the electric field is larger than F_c, the n mixing begins and the quantum number n loses its significance; this is called the strong-field regime, as opposed to the low-field regime where $F\ll F_c$. It is important to keep in mind the n^{-5} scaling law of Eq. (7) because F_c varies extremely strongly with n. The Inglis-Teller limit is on the order of 70 V/cm for $n=30$, but only 0.17 V/cm for $n=100$. Another consequence of the presence of the quantum defects (in other words, of the nondegeneracy of the various l states) is the quadratic Stark effect. If F is low enough, the Stark shift of the nondegenerate states (low-l values) is quadratic. States that have a nonzero quantum defect μ keep their zero-field l character as long as they are outside the hydrogenic manifold, which holds true approximately as long as F is smaller than μF_c. In this regime, nondegenerate states exhibit a quadratic Stark effect. Such behavior occurs for the ns and np series of H_3 (see Sec. V B, below). Then, as F increases, the Stark interaction becomes comparable to the core interaction responsible for the quantum defects and the Stark effect becomes linear. At this point begins the intermediate-field regime, where the behavior of most of the atoms is quasihydrogenic, while typically nonhydrogenic behavior is pronounced at low field.

The position of the classical saddle-point energy determines another important scaling factor. The significance of this point in atomic hydrogen is rather limited because the field-ionization rate [19] and the above-mentioned ionization threshold depend very strongly on $\{n_1,n_2\}$. However, the classical saddle-point energy determines a sharp limit between stable and field-ionized states in nonhydrogenic systems such as H_3 because n_1 and n_2 are no longer exact quantum numbers. This consequence of the breaking of parabolic symmetry is discussed in detail

in a related paper [29] we are preparing that describes the electric-field ionization of H_3. In atomic units, the value of the electric field F_s which corresponds to an effective quantum number n at the saddle point $E_s=-2\sqrt{F}$ is

$$F_s=\frac{1}{16n^4}\ . \tag{8}$$

Note that for any n value larger than 5, F_s is always larger than F_c, and that the ratio F_s/F_c is proportional to n. This means that the relative importance of the strong-field regime increases linearly with n.

We can summarize the four regimes of the Stark effect in a nonhydrogenic system as follows.

(i) Low-field regime: $F<\mu_{\max}F_c$ (where $\mu_{\max}$ is the largest quantum defect). Quadratic effect for the nondegenerate states; l is still a good quantum number if μ_l is large enough (note that in a molecule l is only an approximate quantum number).

(ii) Intermediate-field regime: $\mu_{\max}F_c<F<F_c$. Linear effect; n is conserved but not l (l-mixing region).

(iii) Strong-field regime: $F_c<F<F_s$. Neither n nor l is conserved (n-mixing region), and only m_l is a good quantum number (in a molecule, m_l has no meaning; only M_N, the projection of the total angular momentum N onto the field axis, is conserved).

(iv) Field ionization: $F>F_s$. No stable states.

The influence of the ionic core is not limited to penetration effects. If the Stark interaction is comparable to the energy gap between different core levels, then the structure of the core may influence the Stark spectrum. The coupling scheme between the various angular momenta of the system also plays an important role. In H_3 the energy gap between the ionic levels is large compared to the magnitude of the Stark interaction in the present experiments, but the total angular momentum N of H_3 is not conserved and the coupling between the electronic angular momentum and core rotation is crucial.

Finally, the relative intensities of the transitions to the individual Stark components may also be estimated using the hydrogenic model. For a transition originating from the ground state ($1s$) of hydrogen, the intensity of a $\Delta m=0$ transition is proportional to $(n_1-n_2)^2$ and for $\Delta m=1$ it is proportional to $(n_1+1)(n_2+1)$ (see the general formula in Sec. 65 of Ref. [2]). Thus, in the hydrogenic case, the intensity distribution is parabolic over the Stark manifold for $m=0$ (peaks on the red and blue sides of the manifold, where, respectively, $n_1=0$ and $n_1=n-|m|-1$), while it peaks at the center of the manifold ($n_1\sim n/2$) for $m=1$. Intensities for transitions originating from the $2p$ state, for which no simple analytic formulas are available in the literature, are qualitatively similar except a small local maximum in the middle of the $\Delta m=0$ manifold.

III. EXPERIMENTAL SETUP

The experimental fast-beam apparatus has been described in detail previously [38–41] and is shown schematically in Fig. 1. A fast neutral beam of H_3 molecules is generated by charge transfer of a 1.5-keV H_3^+ beam in cesium vapor. Residual ions are deflected by a small field at the exit of the charge-exchange cell. The charge-transfer process initially produces a wide spectrum of neutral states, but only the rotationless $N=0$ levels (N being the total angular momentum of the molecule, excluding spin) of the $\tilde{B}(2p)^2A_2''$ state are long lived [46], with a lifetime [47] on the order of 700 ns. In this paper, we are only concerned with molecules in the lowest vibrational level of this metastable state; these amount to more than 80% of the total number of neutral in the beam. These molecules are characterized by the quantum numbers $N=K=0$, with symmetric nuclear wave function (ortho-H_3), while the ionic core is characterized by the quantum numbers $N^+=1$ and $K^+=0$.

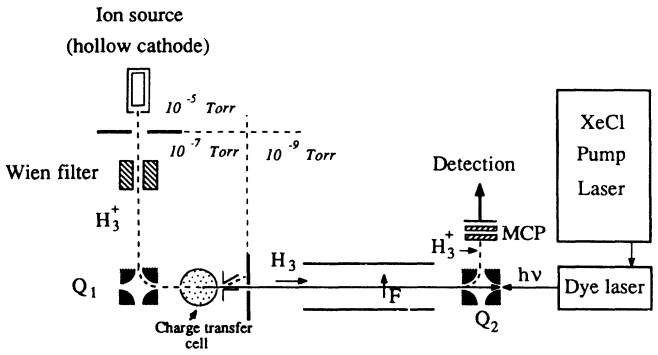

FIG. 1. Experimental setup. The H_3^+ ions produced in a hollow-cathode discharge are mass selected in a Wien filter, deflected in the electrostatic quadrupole Q_1, and then neutralized in the cesium charge-transfer cell. The resulting fast H_3 beam is collinearly excited by the pulsed laser beam. The neutral molecules that are excited but not ionized in the Stark field are field ionized in Q_2, and the H_3^+ ions are detected on a tandem microchannel plate (MCP) and counted during an appropriate time gate.

The fast molecular beam is photoexcited coaxially by an excimer-pumped pulsed dye laser (dye PTP, 338–340 nm) in a region where a well-defined electric field is applied. An electrostatic potential is applied on two parallel metal plates 60 cm long, 5 cm wide, and 24.4 mm apart to produce the Stark field. Along the beam axis between the two plates and over a length of about 45 cm, the homogeneity of the electric field is better than 1%. About 30 cm downstream from the Stark plates, a high value of the electric field is applied in the quadrupole Q_2 (detection field). It ensures that all Rydberg states passing through it with a principal quantum number larger than 30 are field ionized. The resulting H_3^+ ions are energy and mass analyzed in the electrostatic quadrupole (H^+ or H_2^+ fragments are eliminated) and detected on a microchannel plate. The Stark and detection fields are both perpendicular to the propagation of the molecular beam. The neutral beam traverses the interaction region with a velocity of about 3×10^7 cm/s, while the laser-pulse duration is about 10 ns. This arrangement allows us to use the time of arrival of each ion on the detector, measured relative to the laser pulse, to record only the ions produced from a neutral H_3 molecule that was pho-

toexcited in the region where the Stark field is well defined.

A typical "zero-field" excitation spectrum is shown in Fig. 2. In the absence of an external field, owing to the strong p character of the initial state, the excited states are purely nd [38]. This nd series converges toward the first ionization limit [39], 29 562.58 cm^{-1} above the initial state. The ns series is not visible in our spectra because the hydrogenic value of the ratio between $2p \rightarrow ns$ transitions intensity and $2p \rightarrow nd$ transition intensities is almost $\frac{1}{40}$ (see Ref. [2]), and moreover, the ns states are suspected to be affected by rapid predissociation over the entire spectrum.

As described in the preceding section, the relative strength of a given electric field increases as n^5. A field as low as 0.2 V/cm may be considered a very high field for a Rydberg state with a principal quantum number $n=100$. Moreover, as described in Ref. [44], the relative intensities of certain transitions (for example, toward $61d$) are strongly dependent on the field strength at the 0.1-V/cm scale. The question of the definition of the "zero field" is thus of particular importance. Great care was taken to avoid parasite electric fields or external magnetic fields, which, owing to the high velocity of the neutral beam, can generate an appreciable motional electric field. For example, the Earth's magnetic field (about 0.35 G) gives rise to a motional electric field of 0.1 V/cm in the molecular frame. The orientation of the field plates allows us to compensate for this motional field, but other stray fields may still be present. The high-resolution spectrum of Fig. 2 (recorded with a laser equipped with an intracavity Fabry-Pérot étalon), where Rydberg states around $n=125$ are resolved, allows us to assume that the residual field is not larger than the Inglis-Teller limit corresponding to $n=125$, that is, ~ 0.05 V/cm. The limited resolution of our spectrum (about 0.07 cm^{-1}) prevents a more refined estimate of the residual field.

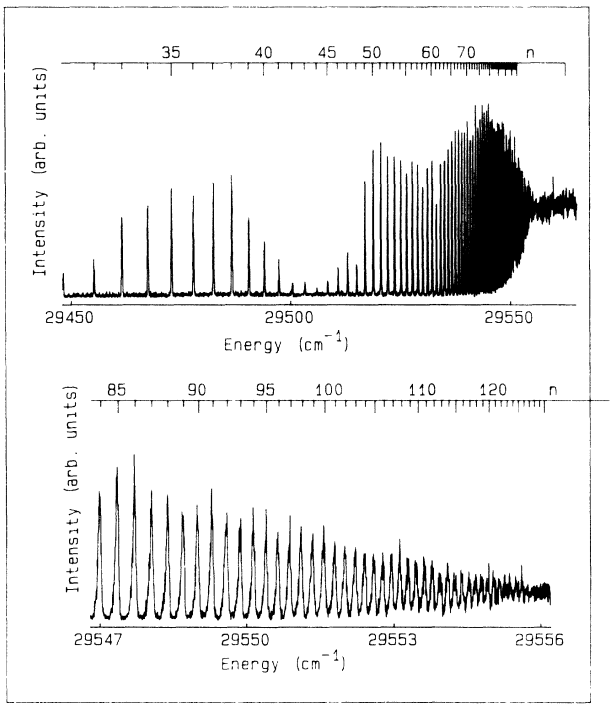

FIG. 2. Zero-field nd-series spectrum. Entire spectrum at low resolution (0.2 cm^{-1}, top) and detail of the high-n region ($n=84$ to ~ 125) at high resolution (0.07 cm^{-1}, bottom). Here and in all our spectra, the energy is measured from the metastable $\tilde{B}(2p)^2A_2''$ ($N=0$) state and n is the principal quantum number relative to the $N^+=1$ ($K^+=0$) ionization limit (29 562.58 cm^{-1}).

IV. EXPERIMENTAL RESULTS

A. Low-resolution spectra

Owing to the field-ionization technique used for detecting the vibrationless Rydberg states, we are not able to monitor the excitation of states with n values lower than 30. The ionizing field is applied perpendicularly to the beam in an electrostatic quadrupole that is simultaneously used as an energy selector. Hence the exposure time to this field is determined by the velocity of the beam and the geometry of the quadrupole. According to our experimental design, the maximum field experienced by the molecules is about 1.8 kV/cm during a few nanoseconds after they enter the quadrupole through a 3-mm aperture. Under these conditions, field ionization is energetically possible for $n>21$, but is efficient only for $n>30$. On the other hand, the molecules excited in the Stark field F between the classical saddle-point energy $E_s=-2\sqrt{F}$ (a.u.) and the zero-field-ionization limit are rapidly ionized and hence deflected in the Stark field, and they are not detected on the microchannel plate. These two characteristics [29] cause the spectra to present a gradual onset on the low-n side around $n\approx 30$ and a sharp drop on the blue side of the saddle-point energy.

Figures 3 and 4 show entire Stark spectra, from $n=30$

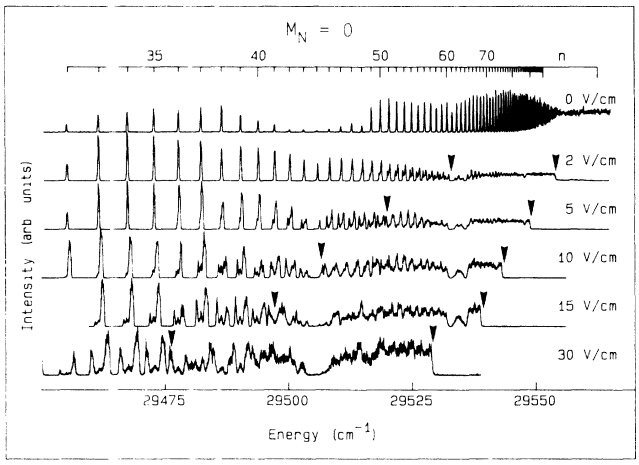

FIG. 3. Entire Stark spectra for $F=0$, 2, 5, 10, 15, and 30 V/cm with $M_N=0$. The arrows indicate the position of the classical saddle-point energy E_s and, at lower energy, the energy E_c (where $F=F_c$) above which n mixing occurs. The windows around $n=40$–48 and at $n=61$ are clearly visible. Note that the $n=40$–48 window almost disappears at $F=2$ V/cm.

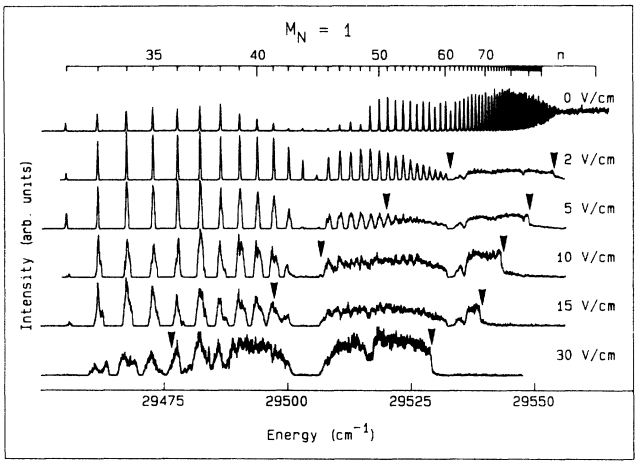

FIG. 4. Stark spectra same as in Fig. 3 except $M_N=1$. Note the different behavior of the windows, especially the wider window around $n=44$.

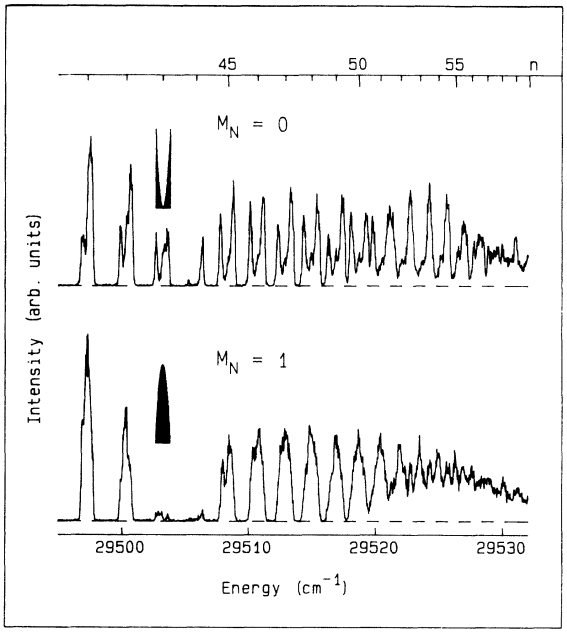

FIG. 5. Expanded view of the $F=5$ V/cm spectra from $n=41$ to 60 with $M_N=0$ (top) and $M_N=1$ (bottom), showing the characteristic shape of the manifold; the minimum is in the center for $M_N=0$, and the maximum is in the center for $M_N=1$. The $n=43$ hydrogenic manifolds for a transition starting from an s initial state are represented in black: top, $m_l=0$; bottom, $m_l=1$.

to the continuum, with, respectively, the laser polarization parallel and perpendicular to the Stark field. The metastable level of the $\tilde{B}(2p)^2A_2''$ state is characterized by $M_N=N=0$. As usual, the field axis is chosen as the quantization axis. If the laser polarization is directed along the field axis, the projection of the total angular momentum remains unchanged and $M_N=0$ in the excited states. Similarly, if the laser polarization is perpendicular to the Stark field, only $M_N=\pm1$ states are excited. Figure 5 shows enlargements of a typical portion of both spectra recorded with a field $F=5$ V/cm, revealing the different aspects of the $M_N=0$ and ±1 spectra.

The spectra in Figs. 3–5 are recorded at a resolution of about 0.2 cm^{-1}. For a typical low-n value (~30) and a field of 30 V/cm, the interval between two adjacent hydrogenic levels (Stark splitting$=3nF$) is on the order of 0.1 cm^{-1}. The field strength at which n mixing begins for $n=30$ is about 70 V/cm. With a resolution of 0.2 cm^{-1}, we could partly resolve the spectra only in the most favorable case of a field $F\approx F_c$ and for the lowest n values. Practically, this limited resolution allows only observation of the envelope of the Stark manifolds. However, much information can be drawn from these unresolved spectra. The position of the saddle-point energy with respect to the zero-field-ionization limit [$E_s=-2\sqrt{F}$ (a.u.) ($-6.11\sqrt{F}$ in cm^{-1}, with F in V/cm)] as well as the position of the critical energy E_c at which the Stark field equals the Inglis-Teller limit F_c [given by Eq. (7)] are indicated in each case. The sharp drop in the spectra at E_s clearly indicates that almost all of the molecules excited above this energy are field ionized during passage through the Stark field. Regarding the critical energy E_c, it is also clear that below E_c each manifold can be distinguished from its neighbor (n is meaningful in this region), while they are merged above E_c (n mixing). As discussed previously, this observation is closely connected to the total width of the Stark manifold, which is measured to have roughly the hydrogenic value ($3n^2F$) at low- and intermediate-field strengths. This last observation, although not surprising, is of some interest, however: It means that no large quantum defect exists which precludes the mixing of all l components in the low-field regime. Even at moderate field, the Stark effect of H_3 is almost hydrogenic. This characteristic is completely different from the case of Na_2, where large quantum defects were responsible for a smaller observed width of the Stark manifold at moderate field [25,32] and a more pronounced nonhydrogenic behavior.

The shape of each manifold, i.e., the distribution of the transition strength as a function of (n_1,n_2), is of particular interest. Note that, although the quantum numbers n_1 and n_2 are not strictly defined in H_3, one can assign such numbers to the various Stark sublevels by correlation with the hydrogenic model. From this point of view, the two spectra in Fig. 5 represent a good example of the intensity variation among members of each n manifold. In the case where $M_N=0$, each manifold presents a maximum intensity on each side, the blue side (high-n_1 values) being more prominent than the red side (low-n_1 values), and a minimum in the middle. In the other case, $M_N=\pm1$, the intensity is greatest in the center and vanishes at the outer wings. The expected shape of the hydrogenic manifold in the case of a $1s\rightarrow(n_1,n_2,m_l=0$ or 1) transition is also represented in Fig. 5 at the position of $n=43$. The similarity between the observed intensity distribution and hydrogenic pattern is striking.

The most important departure from the atomic Stark effect, and the most obviously molecular aspect of our spectra, is observed in the region $n=40$–48 and near

$n=61$, where intensity windows (i.e., regions of the spectra where the ion signal is notably lower than expected) appear. The window formation is strongly field dependent. No trivial channel interactions such as coupling with the rotationally excited series may be invoked to explain any of these windows. This point will be discussed in more detail in Sec. IV C.

B. Partly resolved spectra

We now look for finer details in the H_3 Stark spectra in a region where no obvious perturbations affect the observed intensities. For this purpose, we chose to record high-resolution spectra, using an intracavity Fabry-Pérot étalon to reduce the laser bandwidth to about 0.07 cm^{-1}, in a region where this resolution is finer than the $3nF$ Stark splitting. Such spectra recorded in the vicinity of $n=34$ with $M_N=0$ and ±1 are presented in Figs. 6 and 7, respectively. The Stark field is scanned from 0 to 50 V/cm in increments of 10 V/cm. The Inglis-Teller limit at $n=34$ is about 38 V/cm. Accordingly, the spectra at $F=40$ V/cm show the onset of n mixing: The $n=34$ and 35 manifolds merge, while $n=33$ and 34 are still separated. Below this critical value, the $n=34$ complex is isolated, its simple structure being dominated by the $3nF$ splitting for all field values larger than 20 V/cm, at which value the hydrogenic splitting is resolved. Actually, we will show in Sec. V that, because of the coupling of the electronic angular momentum with the core rotation, each observed line should contain three components. This substructure is not resolved here.

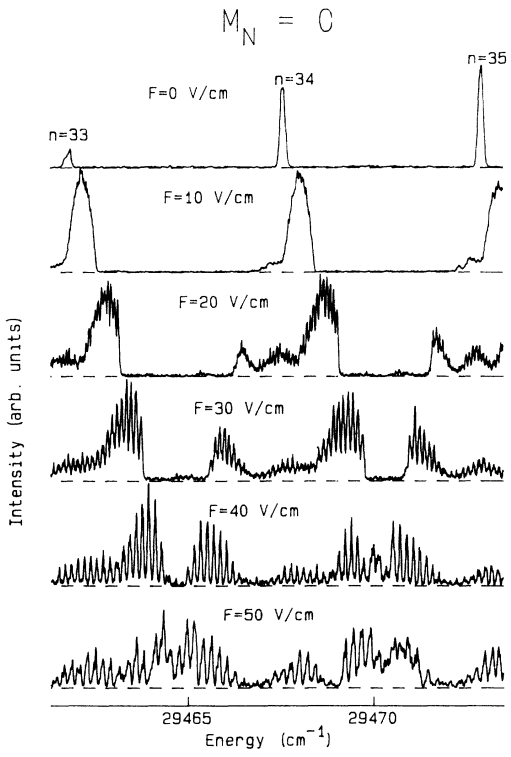

FIG. 6. Stark spectra for $n=33$–35, $M_N=0$, at $F=0$, 10, 20, 30, 40, and 50 V/cm at high resolution (about 0.07 cm^{-1}).

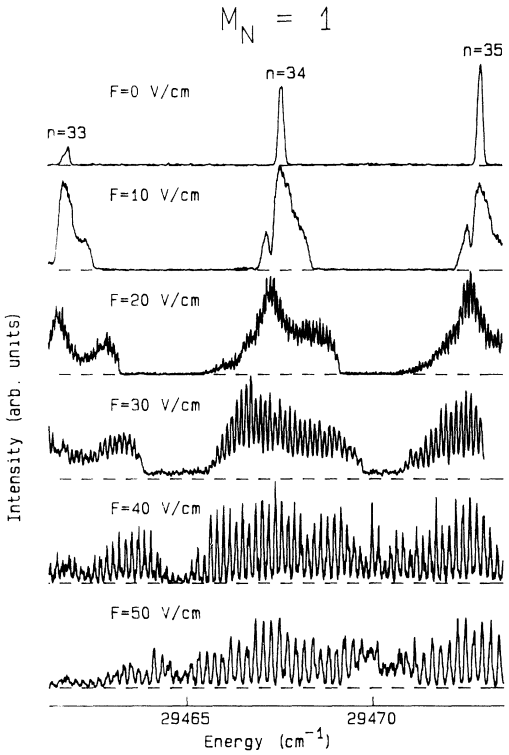

FIG. 7. Stark spectra same as in Fig. 6 except $M_N=1$.

As far as the relative intensities of each individual transition are concerned, the comments made previously apply, with some minor additions. The intensity of the $M_N=0$ states is still maximal at either side of the manifold, although we note that the intensity does not peak at the extreme components. A weak local maximum near the center of the manifold (i.e., near the zero-field energy) is clearly visible in the spectra for $F=20$ and 30 V/cm, in accordance with the expected $2p\rightarrow$high Rydberg intensities in atomic hydrogen. The transitions to the blue states ($n_1>n_2$) are noticeably more intense than those to the red states. This difference is particularly pronounced for $F=10$ V/cm, where the red side is almost entirely missing. When the Stark field is larger than the Inglis-Teller limit (40- and 50-V/cm spectra), this aspect persists except that adjacent manifolds overlap. Similar comments apply to the case where $M_N=\pm1$, except that here the intensity peaks near the center of each manifold. Note that the low-field spectrum (10 V/cm) shows an aberration on the red side of the multiplet in the form of a small hole in the unresolved contour. This extremely localized window has been observed for every manifold in the case of $M_N=\pm1$, and it will be qualitatively explained in the following section.

The relative simplicity and regularity of the spectra displayed in Figs. 3–7 is reminiscent of the Stark spectra of alkali-metal atoms rather than the Stark spectra of alkali-metal molecules [32] such as Na_2 in the sense that rotational structure is absent. The small values of the quantum defects are also responsible for this simplicity. A peculiarity of the H_3 spectra is, however, the appearance of intensity windows, which we discuss below.

C. Windows

The frequent occurrence of window resonances in the bound-state region is probably the most unique aspect of the Rydberg series in triatomic hydrogen. This phenomenon is pronounced in the zero-field spectrum of the *nd* series, as displayed in Fig. 2. The intensities of the transitions in the region from 40*d* to 48*d* is low compared to the neighboring transitions. Transitions toward $n=42$, 43, and 44 are almost absent from the spectrum. In fact, the observed intensities of all transitions below $n=80$ are lower than expected from the $1/n^3$ law, which is obeyed for the high-n members ($n \geq 80$). The window in the region from $n=40$ to 48 is about 25 cm^{-1} wide. At zero-field, this giant window is the most prominent irregularity in the *nd* series in our spectrum, although Ketterle and co-workers [42] observed another giant window in the *nd* series, spanning from $n=12$ to 24. A smaller window [44] is observed in the vicinity of $n=61$, but we attribute its presence in the zero-field spectrum to the stray field, which has been estimated at about 0.05 V/cm. Other windows are also visible near $n=32$, 64, 86, 128,. . . . We have carried out double-resonance depletion experiments, such as described in Ref. [44], in order to measure the absolute absorption intensity of the transitions to *ns* and *nd* states from $n=9$ to 80. These experiments have shown that no local minimum exists in the excitation probability which obeys the $1/n^3$ law. The lack of field-ionizable H_3 molecules at the window positions is therefore only attributable to a dissociative or radiative loss. The time of flight of a H_3 molecule between the optical excitation in the Stark-field region and the field ionization in the detection quadrupole is about 1–2.5 μs. Therefore, if a molecule is excited in a Rydberg state which does not survive this time of flight (either because of predissociation or radiative decay), no H_3^+ signal is detected.

In a previous study [44], we have shown that the $n=61$ window is due to a localized predissociation induced by a vibrational interloper state, the electric field being responsible for mediating the coupling path. Observations of a similar nature have been reported in H_2 where field-induced predissociation is known as being a dominant decay mechanism for many Rydberg states below the ionization threshold [26]. The Rydberg spectra in the vicinity of $n=61$ at low field (0–0.4 V/cm) are displayed in Fig. 8. The intensity of the transition toward $n=61$ is drastically lowered by extremely low fields. The coupling of the $n=61$ state with the dissociative interloper occurs via the *np* series (the window is observed at zero field in the *np* spectrum [37,44]). It is induced by the Stark field through the l mixing. The interloper identified to induce this window is an npE' ($N=0$) state of high vibrational excitation.

The evolution of the broad window near $n=44$ as the field is increased is different from the one at $n=61$ (see Figs. 3 and 4). The window is widely open at zero field, but progressively closes up as the Stark field grows. At $F=2$ V/cm, the window has almost disappeared from the $M_N=0$ spectrum and is limited to the vicinity of $n=44$ in the $M_N=1$ spectrum. At higher-field strengths,

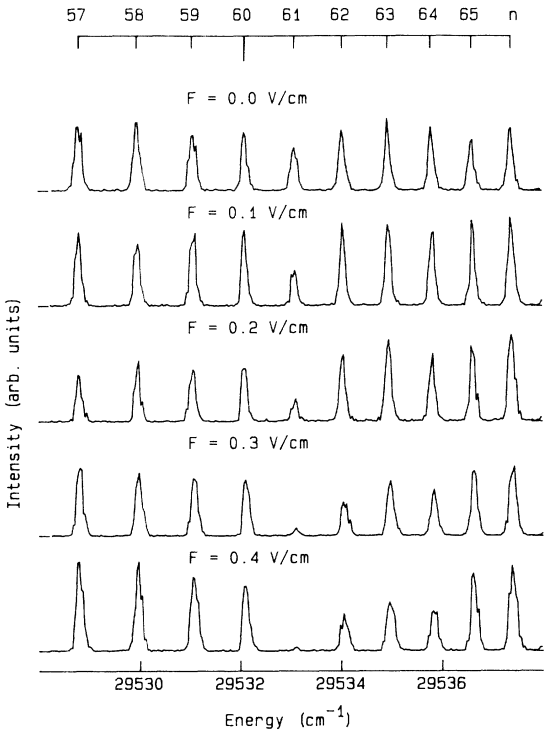

FIG. 8. Low-field (0–0.4 V/cm) *nd* Rydberg spectra around $n=61$, with $M_N=0$ (the appearance of the $M_N=1$ spectra is similar). The disappearance of the $n=61$ line at $F \approx 0.4$ V/cm is caused by field-induced predissociation (see Ref. [44]).

the window reappears and its shape is stable, but still depends on the value of M_N. The high-field limit of the total width of the giant window is about 5 cm^{-1} for $M_N=0$ and 8 cm^{-1} for $M_N=\pm 1$.

We propose the following qualitative explanation for this behavior: In the region $n=40$–48, the *nd* states are coupled to a dissociative interloper, likely a high vibrational level of a low-n Rydberg state in energy near the vibrationless $n=44$ states. Interaction with this interloper at zero field causes accidental predissociation of the neighboring *nd* series members, with a typical lifetime on the order of 1 μs. The coupling required to produce this effect can in fact be exceedingly small. For example, if the lifetime of the interloper state is on the order of 1 ps (corresponding to a width of 5 cm^{-1}), then a contribution by the interloper of only 10^{-6} in the Rydberg wave function is sufficient to induce predissociation on the observed time scale. The coupling has to be weak, because no shift of the *nd* states is observable in the window region. The coupling is almost certainly homogeneous ($\Delta N=0$), and a likely candidate among low excited states of H_3 is the $2s\,^2A_1'$ state, which, for low vibration, has a width of 30 cm^{-1} (lifetime $\tau=170$ fs) [48]. The coupling may, even at zero field, be due to a weak degree of *s-d* mixing induced by the quadrupole moment of the core ion.

In this picture, the coupling between the Rydberg states and interloper state in the window region is controlled by the magnitude of *d* character in each sublevel. This magnitude decreases as the Stark field increases (at least in the sublevels corresponding to the strongest tran-

sitions), thus reducing the coupling strength and width of the window. We will return to this discussion later in this paper after introducing the appropriate Stark map.

The electric field is also responsible for the appearance of other windows around $n=32,64,86,128,\ldots$. Complete discussion and quantitative interpretation of the processes leading to these windows are beyond the scope of this paper and will require a better knowledge of the low-n Rydberg states with high vibrational excitation. In particular, the nature of the dissociative interlopers and of the coupling itself have yet to be investigated.

Nevertheless, the observation of predissociation near the ionization threshold of H_3 may be of great importance for dissociative recombination of H_3^+ with low-energy electrons [49–51] where the stability of highly excited states with respect to dissociative channels is crucial.

V. PERTURBATIVE TREATMENT OF THE MOLECULAR STARK EFFECT

A. Model

The total Hamiltonian of the triatomic hydrogen molecule in a uniform electric field F directed along the z axis is

$$H=H_0-eFz\ , \tag{9}$$

where H_0 is the zero-field total Hamiltonian.

Since the total Hamiltonian of a hydrogen atom in an electric field is separable in parabolic coordinates, the energy matrix of a system having small quantum defects (such as H_3) is almost diagonal in the parabolic basis $\{n_1,n_2,m\}$. However, because of the small non-Coulombic terms in the Hamiltonian H_0 and the presence of the core angular momentum, it is not convenient to derive the expressions for the diagonal and small off-diagonal terms of the energy matrix in the parabolic basis. The formal derivation of these matrix elements is straightforward in the usual spherical basis $\{n,l,m\}$, which has been systematically used in similar calculations in atomic physics [4,14,16]. The ease of calculating the matrix elements compensates for the lack of the symmetry of the hydrogenic Stark effect and the separability in parabolic coordinates.

In the spherical basis that diagonalizes H_0, the diagonal elements of the energy matrix are obviously the eigenvalues of the Hamiltonian H_0 (zero-field energies), while the off-diagonal terms contain only the contribution of eFz. A simplification arises from the fact that, in H_3 and zero field, all the high Rydberg states except the np series are well described using a pure Hund's case d basis. That is, the rotational quantum number of the ionic core (N^+) is a good quantum number. Of course, N^+ is not affected by the optical (electronic) excitation and has the same value as in the initial $\tilde{B}(2p)^2A_2''$ state: $N^+=1$ ($K^+=0$). The l uncoupling in the np [37], nd [38,39], and nf [40] series has already been studied in detail. The mixing in N^+ introduced by the l uncoupling is completely negligible for $l\geq 2$ where all quantum defects are smaller than 0.02, and it is not relevant to the case where $l=0$. In addition, the separation $\Delta E_{\rm rot}$ between the $N^+=1$ ($K^+=0$) and $N^+=3$ ($K^+=0$) levels (because of proton-spin statistics, there is no even N^+ level with $K^+=0$) is far larger than the highest Stark matrix element corresponding to our experimental conditions. In atomic units, the magnitude of this matrix element is $3n^2F$, while the maximum field to be considered is the ionizing field $F_s=1/16n^4$, above which no stable states are observed. That is, the maximum matrix element is $3/16n^2\leq 45\ \text{cm}^{-1}$ for $n>30$. Even in the worst case, this term is one order of magnitude smaller than $\Delta E_{\rm rot}=429.9\ \text{cm}^{-1}$. The effect of the Stark field on the electronic orbitals of H_3^+ is therefore negligible at the fields considered here. These considerations allow us to set $N^+=1$ ($K^+=0$) in our perturbation basis.

However, the l uncoupling in the np series is not negligible and is responsible for appreciable mixing of the $np(N=2,N^+=1)$ series with the core-excited $np(N=2,N^+=3)$ Rydberg series. The rotational mixing is particularly strong in the vicinity of the $n=15$ member of the $N^+=3$ series, which quite coincidentally lies in the region of the giant window resonance $n\approx 40$–48. Since this mixing is limited to the $np(N=2)$ series and the $n=15(N^+=3)$ state is almost unaffected by the fields considered here ($3n^2F\approx 1.4\ \text{cm}^{-1}$ at $F=50$ V/cm for $n=15$, compared with a 14–15 splitting of about 70 cm^{-1}), we introduce N^+ mixing in the energy matrix phenomenologically and neglect the marginal contribution of the $N^+=3$ component in the off-diagonal elements. The energy and amplitude of the $N^+=1$ component of the wave function are both calculated using a two-channel quantum-defect theory described in Ref. [37]. The $N=0$ and 1 np series are not perturbed by any rotational interaction and are purely $N^+=1$.

Because the electric field breaks the spherical symmetry, all the l values ($l\leq n-1$), and consequently all the N values, must be included in the perturbation basis, with the restriction

$$\mathbf{N}^+ + l = \mathbf{N}\ . \tag{10}$$

Owing to the unique value of $N^+=1$, the perturbation basis is limited to the values $N=l$ or $l\pm 1$ if $l\neq 0$ and $N=1$ if $l=0$.

The diagonal elements of the energy matrix are calculated with the Rydberg formula using the quantum defects μ_l (see Tables I and II). For $l\neq 1$,

$$H_0^{nl}=E_{\rm ion}-\frac{\mathcal{R}}{(n-\mu_l)^2}\ , \tag{11a}$$

and for $l=1$,

$$H_0^{npa_2''}=E_{\rm ion}-\frac{\mathcal{R}}{(n-\mu_{pa_2''})^2}\quad (N=0)\ , \tag{11b}$$

$$H_0^{npe'}=E_{\rm ion}-\frac{\mathcal{R}}{(n-\mu_{pe'})^2}\quad (N=1)\ , \tag{11c}$$

and $H_0^{n^*(N=2)}$ is calculated using a two-channel quantum-defect theory [37]. $E_{\rm ion}$ is the first ionization limit [39] of H_3 ($N^+=1$, $K^+=0$ vibrationless level of the

TABLE I. Effective quantum defects of the low-ns A_1' states.

	Effective quantum defect				
	a	b	c	d	e
$2s\ a_1'$	0.0836	0.08	0.08		
$3s\ a_1'$	0.0706	0.07	0.07	0.080	
$4s\ a_1'$	0.0663	0.05	0.05		
High n's					0.075

[a]King and Morokuma [33].
[b]Jungen [52].
[c]Martin [53].
[d]Lembo, Helm, and Huestis [41].
[e]Ketterle and co-workers [42].

ground state of the H_3^+ ion) and equals 29 562.58 cm^{-1} when measured from the initial metastable state. $\mathcal{R}$ is the Rydberg constant for H_3 and equals 109 717.40 cm^{-1}. The values of the quantum defects used in our calculation are reported in Tables I and II. Table I lists calculated [33,52,53] and measured [41,42] values of the ns-series quantum defects of low Rydberg states. High Rydberg states of the ns series ($n > 30$) are not known and are not visible in our spectra, partly because of the low intensity of the $2p \rightarrow ns$ transition as compared to $2p \rightarrow nd$ (hydrogenic value of the intensity ratio $\approx \frac{1}{40}$) and partly because of the strong predissociation that is suspected to affect this series [42].

The np-, nd-, and nf-series quantum defects have been measured [37–40] in our group for $n > 30$ and are reported in Table II. Comparisons with low-n calculated effective quantum defects show a remarkable agreement between experiment and theory. Such an agreement must be emphasized because it is not very frequent in molecular physics and it is encouraging for further use of results of *ab initio* calculations. Finally, the quantum defects of the high-l series are assumed to be zero ($\mu_{l>3}=0$).

By using the Wigner-Eckart theorem and the general expression for the reduced matrix element of the product of two operators [54], the off-diagonal matrix elements of the total Hamiltonian may be expressed in the spherical basis as

$$H_{nl,NM_NN^+}^{n'l',N'M_{N'}N^{+\prime}} = -eF\langle nl,NM_NN^+|z|n'l',N'M_{N'}N^{+\prime}\rangle$$

$$= -eF(-1)^{N-M_N+l+N^++N'} \begin{pmatrix} N & 1 & N' \\ -M_N & 0 & M_N \end{pmatrix} \begin{Bmatrix} l & N & N^+ \\ N' & l' & 1 \end{Bmatrix} \sqrt{(2N+1)(2N'+1)}$$

$$\times \sqrt{l_{\max}} R_{nl}^{n'l'} \delta(N^+,N^{+\prime}) \delta(M_N,M_{N'}) \delta(l',l\pm 1) , \tag{12}$$

where $l_{\max}$ is the larger of l and l'.

The selection rules for the matrix element (12) are $l'=l-1$ or $l+1$, $M_{N'}=M_N$, $N'=N$ or $N\pm 1$, $N^{+\prime}=N^+=1$, and $K^{+\prime}=K^+=0$ (the last two selection rules are a consequence of the negligible effect of the Stark field on the core ion).

The radial integral $R_{nl}^{n'l'}$ is

$$R_{nl}^{n'l'} = \int_0^\infty R_{n'l'}(r) r R_{nl}(r) r^2 dr , \tag{13}$$

where $R_{nl}(r)$ represents the hydrogenic radial function and where n can take noninteger values. The generalized Coulombic integral is calculated with the help of the numerical method proposed by Edmonds *et al.* [55]. In this integral, the principal quantum number is replaced by the effective zero-field quantum number $n^*=n-\mu_l$. The magnitude of the radial integral oscillates and decreases rapidly as $n^*-n'^*$ increases. No strict selection rule or simple approximate formula for $R_{nl}^{n'l'}$ exists when the difference $n^*-n'^*$ is not an integer and numerical evaluation of Eq. (13) is required. This term is directly respon-

TABLE II. Calculated and measured quantum defects of the np, nd, and nf Rydberg series of H_3. The quantum defect of the nd series quoted in column d is the effective quantum defect of the nd $N^+=1$ series (same comment applies to the nf series), which is an admixture of a_1' and e' symmetries. Considering the uncertainties in the experimental values of the quantum defects (≈ 0.02), the agreement between calculated and experimental values is excellent.

	Quantum defects			
Orbital symmetry	a	b	c	d
$np\ e'$	0.3380	0.35	0.34	0.39
$np\ a_2''$	0.0244	0.02	0.00	0.05
$nd\ e'$	0.0236	0.02	0.02	
$nd\ e''$	−0.0047	−0.04	−0.01	0.019
$nd\ a_1'$	−0.0134	−0.02	−0.02	
nf				0.012

[a]King and Morokuma [33].
[b]Jungen [52].
[c]Martin [53].
[d]Our results: np series [37], nd series [38,39], and nf series [40].

sible for the coupling between the different n manifolds. This fundamental difference from atomic hydrogen is especially sensible when the energy gap between levels arising from different n manifolds is small, as, for example, in the n-mixing region, where one has to include several n values in the perturbation basis. Comparing Eqs. (12) and (13) with similar formulas for the case of atomic helium [14] shows the striking similarity between the molecular and atomic coupling schemes. The expression of the off-diagonal Stark matrix element in atomic helium is similar to the one given by Eq. (12) if one replaces the core-electron, Rydberg-electron, and total electronic angular momenta in helium (l_1, l_2, and L) with the core angular momentum N^+, the Rydberg-electron angular momentum l, and the total angular momentum (excluding spin) N of H_3, respectively.

To compare our calculation with our experimental results, it is necessary to calculate the intensity of excitation—or absorption intensity—of the Stark state from the initial low-lying metastable state. The oscillator strength for a transition from the initial state $|\tilde{B}(2p), N=0\rangle$ to a Stark state $|E, M_N\rangle$ is

$$f_{B,E} = \left| \sum_{E',l',N'} C^E_{E'l'N'M_N}(F) \times \langle \tilde{B}2p, N=0|\varepsilon r|E'l'N'M_N\rangle \right|^2 , \quad (14)$$

where the term $C^E_{E'l'N'M_N}(F)$ represents the components of the $|E, M_N\rangle$ state in the perturbation basis. The matrix element involved in Eq. (14) is easily separated into an angular and a radial part. Obviously, the sum over l' is limited to $l'=0$ or 2, the former being almost negligible compared to the latter. The angular part is trivial. Starting from an initial state with $N=0$, only $N=1$ terms have a nonzero contribution. The radial part is more delicate to estimate. The Coulombic approximation, even generalized to noninteger values, is not well suited for accurate calculation of matrix elements involving a low-lying state, especially in the case of a molecular core, because the integral is sensitive to the small-r part of the wave function. However, it can give accurate relative values for the various Rydberg states [4].

The number of terms in a given n manifold of our perturbation basis is $3n-2$ when $M_N=0$ or $3n-3$ when $M_N=1$ (there is no $N=0$ state in that case). Combining these terms with the large-n values of the observed Rydberg states leads rapidly to a large size for the matrix that has to be diagonalized. To avoid excessive size, we must truncate our perturbation basis to a limited range of n values. We chose to limit ourselves to field values not too much larger than the Inglis-Teller limit where n mixing begins. Without making a large error in calculating the n manifold (probably less than 0.1 cm^{-1}), we can rely on a calculation that includes the $n-1$, n, and $n+1$ terms to calculate the n manifold. The $n-1$ and $n+1$ levels are not necessarily correctly computed, and only the central manifold is correct. This is valid as long as the $n-2$ and $n+2$ manifolds are not too close to the n manifold, i.e., for field values not larger than about $1.5F_c$. With this restriction, the size of the Hamiltonian matrix is $9n_0-6$ for $M_N=0$ and $9n_0-9$ for $M_N=1$. A typical matrix dimension is about 350 for $n\sim40$. Of course, there is no fundamental obstacle (other than the computer capabilities) to including more n components in the basis if a higher accuracy is needed or if the field strength greatly exceeds the Inglis-Teller limit.

Figure 9 shows an example of such a model calculation using the quantum defects listed in Tables I and II for the $n=10$ manifold and an electric field $F=8$ kV/cm (about one-half of F_c). We chose this low-n value for clarity, because then the number of Stark states is small. We recognize the splitting of the $n=10$ manifold into groups of lines. The hydrogenic levels which are separated by $3nF$ are indicated at the top of each model spectrum, and it is possible to establish a correlation between these hydrogenic levels and each group of lines of the H_3 calculated Stark manifold. Each group corresponds to a particular value of the parabolic quantum numbers (n_1, n_2) in the hydrogenic limit and is composed of three transitions corresponding to three different dominant values of the total angular momentum N. Only the $N=1$ amplitude contributes to the intensity of the transition, and generally only one of these three sublevels bears the dominant oscillator strength.

Several differences between the $M_N=0$ and 1 spectra are visible in this model calculation. First, as stated before, the line intensity is maximal for $n_1\approx0$ or n when $M_N=0$, while the $n_1\approx n/2$ lines are the most intense when $M_N=1$. Second, the shift with respect to the hydrogenic position is important, especially at the field strength used in Fig. 9, where one sublevel (np, $N=1$) is still outside the hydrogenic multiplet. Finally, the splitting between individual lines within each group of lines labeled as having the same value of n_1 is strongly dependent on n_1 and M_N, and it evolves irregularly with the

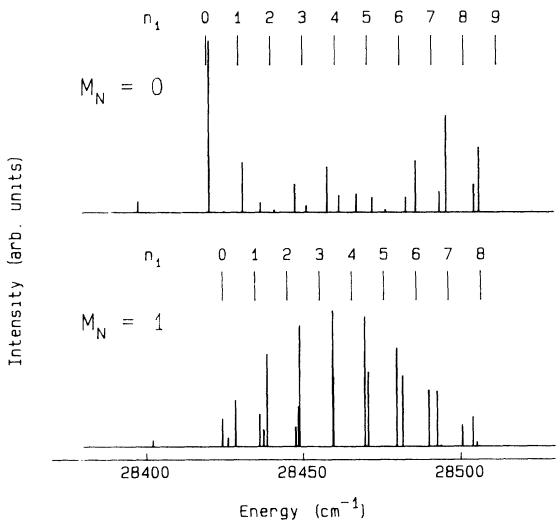

FIG. 9. Model calculation for $n=10$, $F=8000$ V/cm, and $M_N=0$ (top) and 1 (bottom). The markers labeled $n_1=0,1,2,\cdots$ represent the hydrogenic Stark states. Note the splitting of each n_1 line into three lines (only one may be visible in some cases).

field strength (see also the Stark maps in Sec. IV B). Unfortunately, this typical molecular "fine structure" due to the l-N^+ coupling is too narrow in the case of Rydberg states $n > 30$ to be resolved in our spectra, and we will not investigate this aspect further.

B. Comparison with experiment

In comparing the theoretical predictions with the experimental spectra, one must keep in mind that the model we use does not account for any decay process of the Rydberg states following their excitation. As we shall see, the predissociative decay of selected window regions of the spectrum discussed above also inflicts a selective loss of those Stark states that contain a substantial amplitude of low-l character.

Calculated spectra convoluted with an experimental width of 0.07 cm^{-1} are displayed in Figs. 10 and 11. These calculations correspond to the experimental conditions of Figs. 6 and 7, i.e., $n=34$, $F=0-50$ V/cm, and $M_N=0$ and 1, respectively. Comparison of Figs. 6 and 10 and Figs. 7 and 11 shows a satisfactory agreement between calculation and experiment, especially in the case of high-field values where the n mixing is well accounted for by our model. A more direct comparison of experimental and theoretical spectra for the $n=34$, $M_N=0$ manifold is presented in Fig. 12 for $F=10$, 20, 30, and 40 V/cm. The quantum defects used in these calculations were chosen according to the zero-field experimental re-

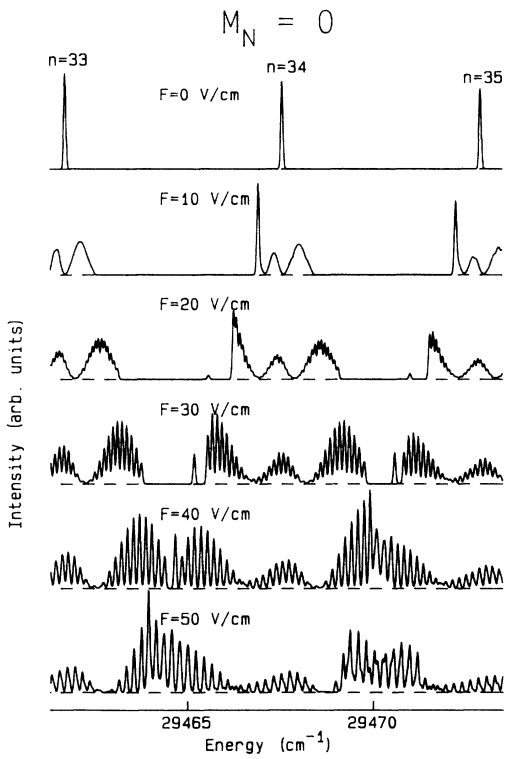

FIG. 10. Calculated Stark spectra for $n=33-35$, $M_N=0$, at $F=0$, 10, 20, 30, 40, and 50 V/cm. Compare with experimental data in Fig. 6. Calculated lines are broadened to an experimental width of 0.07 cm^{-1}.

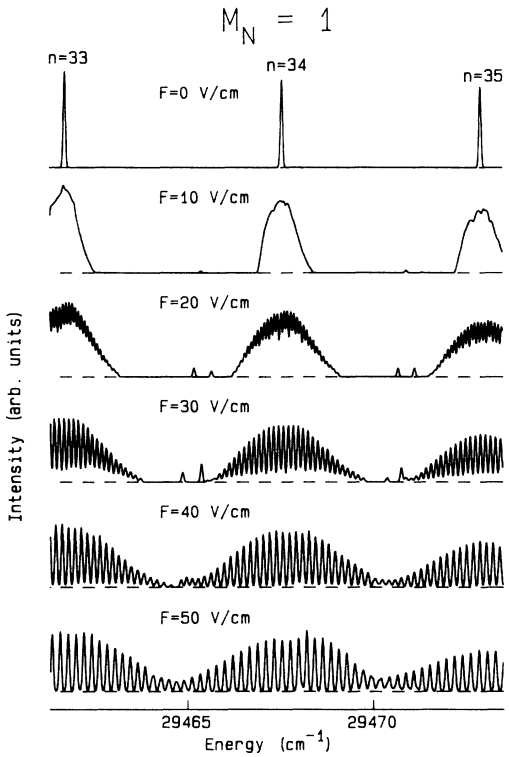

FIG. 11. Calculated Stark spectra in the vicinity of $n=34$, $M_N=1$, at $F=0$, 10, 20, 30, 40, and 50 V/cm. Compare with experimental data in Fig. 7.

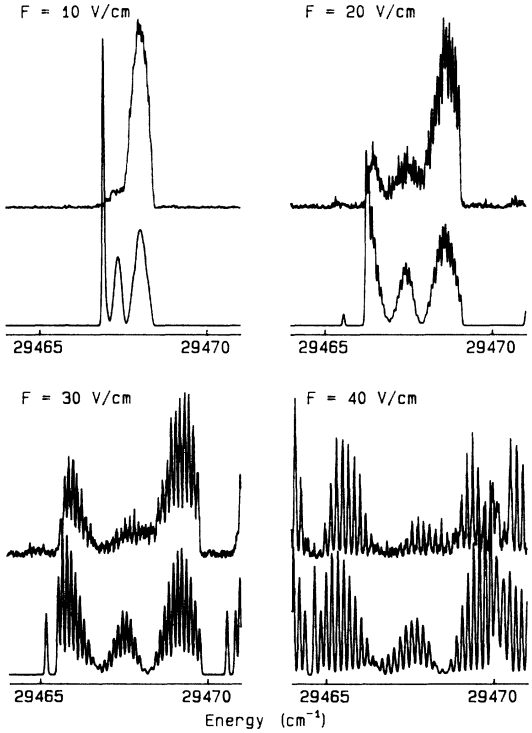

FIG. 12. Direct comparison of experimental and calculated spectra for $n=34$, $M_N=0$, and $F=10$, 20, 30, and 40 V/cm. In each case, the calculated spectrum (bottom trace) is superimposed on the experimental one (top trace; all intensities are in arbitrary units). Low-n_1 lines (red "wings" of the manifolds) are clearly missing from the experimental spectra, especially at moderate fields.

sults (Tables I and II). The following parameters were used:

$$\mu_s=0.07,\quad \mu_{pa_2''}=0.05\ ,$$

$$\mu_{pe'}=0.39,\quad \mu_d=0.02\ ,$$

$$\mu_f=0.01,\quad \mu_{l>3}=0.00\ .$$

Let us first discuss the $M_N=0$ spectra (Figs. 6, 10, and 12). The agreement between calculated and experimental line positions is excellent and is generally better than the experimental precision. This agreement is particularly evident in Fig. 12. Note, however, that since only the $n=33$, 34, and 35 terms are included in the calculation, only the $n=34$ manifold is predicted correctly. Small discrepancies in the $n=33$ and 35 manifolds occur owing to the absence of the $n=32$ and 36 manifolds in the perturbation basis.

Nevertheless, especially at low fields (10 and 20 V/cm), the intensities of the low-n_1 components (red side of the manifold)—or the low-l components since the ns and np states are located on the red side of the multiplet—are predicted to be much stronger than those observed in our spectra. This discrepancy diminishes as the field increases and as the particular l character of these low-n_1 components is diluted throughout the manifold. It is important to note that, at low and moderate fields, states on the red side of the manifold have still one (or two) relatively dominant l components. Indeed, of all the l states, only the s and p states have quantum defects larger than 0.05. Hence, as long as the field is not too strong, the low-n_1 states possess strong s and p components and thus acquire to an appreciable degree the character of these low-l states. This is manifest on the $M_N=0$ Stark map displayed in Fig. 13. The nondegenerate states are, starting from the lowest-term value, $34p(N=1)$, $34p(N=2), 34s(N=1), 34p(N=0),\ldots$. These states are initially isolated from the hydrogenic multiplet and thus retain approximately their l character until field values of about 40 V/cm are reached for the $34p$, $N=1$ and 2 states, and about 10 and 5 V/cm for the $34s(N=1)$ and $34p(N=0)$ states, respectively. Note that $34p(N=1)$ and $34p(N=2)$ states show an avoided crossing near $F=32$ V/cm, indicating the stronger coupling of the $p(N=2)$ states to the other l states.

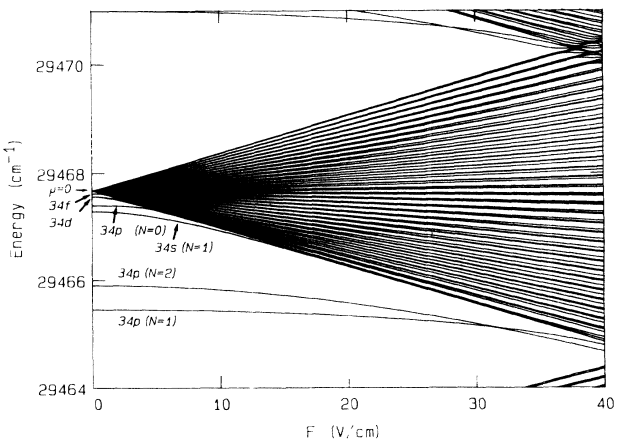

FIG. 13. Calculated Stark map for $n=34$, $M_N=0$, and field values (F) ranging from 0 to 40 V/cm. The $34p(N=0)$, $34s(N=1)$, $34p(N=2)$, and $34p(N=1)$ states are merged with the rest of the manifold at field strengths of about 5, 10, and 40 V/cm, respectively. Below these values, they exhibit the characteristic quadratic Stark effect. Note the avoided crossings between the $N=1$ and 2 $34p$ levels and between the $n=34$ and 35 manifolds.

Assuming the unstable character of the low-l states (and especially the s states) with respect to predissociation, this picture explains qualitatively the lack of field-ionization signal, which appears on the red side of the manifold in terms of a loss of population via predissociation and possibly radiation. We expect that if the Stark spectra were recorded in absorption, no such loss would occur. The selective loss of states with appreciable s or p character is attributed to the fact that s and p states are the more penetrating (origin of their fairly large quantum defects); thus they are the most sensitive to interaction with the core and particularly to predissociation. On the other hand, if the electric field is strong enough (on the order of F_c), no particular l component dominates in any level and the coupling to the decay channels is diluted, afflicting equally all Stark levels.

If we now compare the $M_N=1$ spectra (Figs. 7 and 11), we find that similar conclusions can be drawn: The line positions are well reproduced, but the calculated intensities of the low-n_1 components are too strong. Although the experimental manifolds are less regular than the calculated ones with respect to the distribution of the observed intensity, the agreement is better than in the $M_N=0$ case. This is obviously a consequence of the low-n_1 components, which are the most affected by predissociation, corresponding to the weakest transitions when $M_N=1$.

However, a particular departure of the experimental spectrum from the theoretical predictions is seen in the $M_N=1$, $F=10$ V/cm spectra (see Fig. 7). At an energy of 29 467.30 cm^{-1}, the intensity of the $n=34$ manifold shows a significant drop in the unresolved experimental contour. Such extremely localized windows may be seen for many n values at comparable relative positions and field strengths. Examination of the detail of the $M_N=1$, $n=34$ Stark map in Fig. 14 suggests the following explanation. Starting from the lowest-term value, the $M_N=1$ states are $34p(N=1)$, $34p(N=2)$, $34s(N=1)$, and $34d(N=1,\ 2,$ and $3)$. The $np(N=0)$ state is absent from the $M_N=1$ Stark map. A consequence of its absence is that the $ns(N=1)$ state couples in first order only to states that are located lower in energy. Thus the ns state is repelled toward higher energy by the np states and it crosses a large part of the $n=34$ manifold [indicated by a dashed line in Fig. 14(b)]. Indirect couplings via the p states result in the crossings being avoided, but the computed wave function shows that the s component largely dominates near the crossing, revealing that the s state preserves its character while embedded in the high-l states as long as the np states are isolated from the rest of the manifold. This holds true until a field value of about 30 V/cm for $n=34$. Note that $34p(N=1)$ and

$34p(N=2)$ do not cross when $M_N=1$. At $F=10$ V/cm, the predicted position of the quasi-s-state that crosses half of the manifold is 29 467.34 cm^{-1} (its s component is 0.75; i.e., this state has more than 50% s symmetry), which corresponds with good accuracy to the energy where we observe the small hole in the ionization signal. This example suggests that the embedded s state inflicts selective predissociation to the neighboring Stark states in accordance with the arguments invoked previously. It may also explain the different width of the window around $n=44$ depending on M_N, at least at intermediate-field strengths, because the quasi-s-state is closer from the state having the largest excitation amplitude when $M_N=1$.

Taking into account the calculated amplitude of the s component and estimating empirically the lifetime of the zero-field ns state, we could, in principle, reproduce this effect phenomenologically. However, most of the states that have a strong s component also have a small nd component and thus should not dominate the observed intensity. For this reason, simulation of the s-coupling-induced predissociation based on this simple model is precluded. Previous results for the np series [37], coupled in first order to the nd series that bears all the oscillator strength, have shown that predissociation of np states is localized and is not the general case, as opposed to what we believe about the ns series. Thus, in addition to the mechanism caused by the field-induced mixing with the s states, one has to assume that the d states possess a small amount of s character even in zero field. Therefore, it appears that s-d mixing would also have to be accounted for if one wishes to understand the dynamics of these Rydberg states. A non-negligible s-d mixing rate supports the observation of the giant window caused by a low-ns interloper around $n=40-48$ and the relatively low intensity of nd states below $n=40$. Indeed, even if the s-d mixing is constant over the entire Rydberg region, we expect the lifetime to evolve as $1/n^3$, which could explain why the evolution of the observed line intensities in the nd series is not in agreement with the $1/n^3$ law, the high-n lines being relatively stronger than the low-n lines.

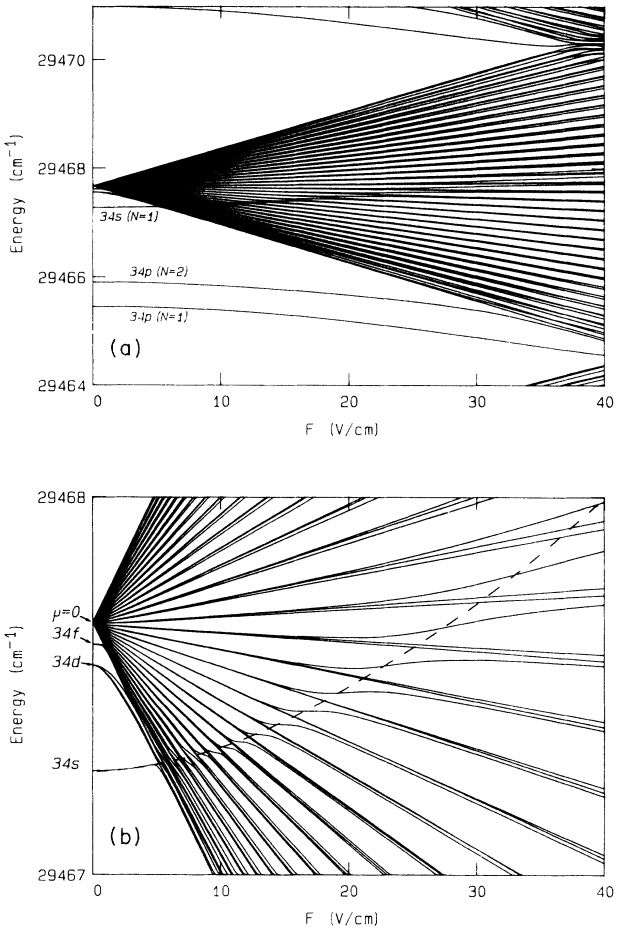

FIG. 14. (a) Calculated Stark map for $n=34$, $M_N=1$, and field values (F) ranging from 0 to 40 V/cm. (b) Detail showing the evolution of the s state as it is repelled through the manifold (dashed line) by the lower-lying np states. Note that only one "fine-structure" component of each n_1 Stark state follows and avoided crossing with the $34s(N=1)$ state.

Perturbation theory has proved here to be a very powerful tool for predicting the energy levels and redistribution of oscillator strength among the Stark states. Comparing the observed field-ionization intensity and calculated absorption intensity gives a qualitative idea of the magnitude of the coupling of the Rydberg states to the dissociative states. Moreover, this comparison has allowed us to distinguish between two fundamentally different decay processes: (1) rovibrational interactions with low-n interlopers with several quanta of vibration, leading to accidental predissociation and apparently randomly distributed window resonances, and (2) preferential decay of states that acquire s character.

A further step in reconciling theory and experiment could be to resolve the internal structure of each n_1 component. More precise information about electron-core couplings could be extracted from such spectra, and there is no doubt that direct observation of this yet unobserved molecular Stark structure would reveal interesting features about the dynamics of molecular Rydberg states in an electric field.

C. Perturbative treatment versus MQDT

The above results demonstrate that the classical perturbative treatment gives correct results for calculating the energy positions and intensities of Stark spectra of H_3 Rydberg states. Deviations appear when l-selective decay channels remove the population in specific Stark states before they are detected. The single important approximation, that the core remains in its ($N^+=1$, $K^+=0$) vibrationless level and is not affected by the external field, is easy to accept in H_3 and does not falsify the calculated energy levels. Owing to its simple formalism, perturbation theory is clearly well suited for this purpose in cases where the perturbation basis does not become immoderately large.

We could have used a multichannel quantum-defect theory such as those described by Sakimoto [23] for H_2 or by Brevet *et al.* [25] for Na_2. The MQDT formalism has the advantages that it benefits from the separability of the

hydrogenic problem in parabolic coordinates and reduces the size of the calculation basis, which renders MQDT extremely powerful in situations where angular couplings are complex and where a prohibitive number of channels (or basis vectors) would have to be included in a perturbative method. The MQDT formalism allows also in principle the calculation of the spectra above the ionization threshold in the region where no discrete states exist. However, in the high-field regime, application of MQDT requires calculation of several elliptic integrals at each step of energy; the simple and elegant analytic hydrogenic formulas can only be used in the low-field regime.

In the particular case of H_3, where the limited number of core states (only $N^+=1$, $K^+=0$) leads to a relatively modest perturbation basis, the perturbative method presented here is clearly a good choice and the results obtained here substantiate our claim. Nevertheless, for a heavier molecule, where many rotational channels participate, the size of the perturbation problem may become problematic. Thus far, however, MQDT treatment of the molecular Stark effect in H_2 or Na_2 is only fragmentary, while the present perturbative treatment is carried through completely and requires no adjustable parameters.

Considering these arguments, the perturbative treatment is clearly useful in understanding the coupling schemes and relative orders of magnitude of the interactions involved in the molecular Stark effect. It has also proved to be very powerful in substantiating the very selective predissociations that affect the *s* and *p* states at such high electronic energies.

VI. CONCLUSION

Stark spectra of high Rydberg states ($n=30-125$) of triatomic hydrogen have been obtained at low- and high-field strengths, and the observed Stark structures have been analyzed using perturbation theory where only minor approximations have to be made. Experimental zero-field data (quantum defects) have been used, and despite the absence of fitting parameters, the agreement between theory and experiment is highly satisfactory. This result is remarkable in the sense that it is the first complete quantitative perturbative treatment of molecular Rydberg states in an external field.

Comparison of the experimental spectra with the predictions of the perturbative treatment also revealed field-induced predissociation. A more complete analysis of this effect will require a more thorough understanding of the highly excited vibrational states of H_3, their coupling to the vibrationless states presented in this paper and their coupling to the repulsive ground state of H_3. From this point of view, recent findings about the vibrationally excited levels of the ground state of the H_3^+ ion [56] and detailed calculation of the potential surfaces of some Rydberg states [57] are encouraging. The process leading to the apparent systematic predissociation of the *ns* states as well as the magnitude of the *s-d* mixing will also have to be examined in more detail.

We expect that a quantitative understanding of the Stark effect in highly excited molecules can teach us about the influence of the electric field on the molecular dynamics and about the hypothetical quantum chaos, for which a molecule in a field is a privileged system.

ACKNOWLEDGMENTS

It is a pleasure to acknowledge fruitful discussions with Dr. D. L. Huestis of SRI. This research was supported by the U.S. Air Force Aero Propulsion Laboratory, Wright Patterson Air Force Base, under Contract No. F 33615-90-C-2007. One of us (C.B.) wishes to thank NATO for support. The Laboratoire de Spectrométrie Ionique et Moléculaire is "Unité Associée au Centre National de la Recherche Scientifique No. 171."

*Permanent address: Laboratoire de Spectrométrie Ionique et Moléculaire, Université Claude Bernard Lyon I, 43 Bd. du 11 Novembre 1918, 69622 Villeurbanne CEDEX, France.

[1] E. Schrödinger, Ann. Phys. (Leipzig) **80**, 437 (1926).

[2] H. A. Bethe and E. E. Salpeter, *Quantum Mechanics of One- and Two-electron Atoms* (Plenum, New York, 1977).

[3] L. D. Landau and E. M. Lifshitz, *Quantum Mechanics, Non-Relativistic Theory,* 3rd ed. (Pergamon, New York, 1976).

[4] M. L. Zimmerman, M. G. Littman, M. M. Kash, and D. Kleppner, Phys. Rev. A **20**, 2251 (1979).

[5] C. Fabre, P. Goy, and S. Haroche, J. Phys. B **10**, L183 (1977); C. Fabre, Y. Kaluzny, R. Calabrese, Liang Jun, P. Goy, and S. Haroche, *ibid.* **17**, 3217 (1984).

[6] C. Chardonnet, F. Penent, D. Delande, F. Biraben, and J. C. Gay, J. Phys. (Paris) **44**, L-517 (1983).

[7] D. Tuan, S. Liberman, and J. Pinard, Opt. Commun. **18**, 533 (1976).

[8] R. R. Freeman and N. P. Economou, Phys. Rev. A **20**, 2356 (1979).

[9] J. M. Lecomte, S. Liberman, E. Luc-Koenig, J. Pinard, and A. Taleb, Phys. Rev. A **29**, 1929 (1984).

[10] H. Rinneberg, J. Neukammer, G. Jönsson, H. Hieronymus, A. König, and K. Vietzke, Phys. Rev. Lett. **55**, 382 (1985).

[11] D. E. Kelleher and E. B. Saloman, Phys. Rev. A **35**, 3327 (1987).

[12] A. Nussenzweig, E. E. Eyler, T. Bergeman, and E. Pollack, Phys. Rev. A **41**, 4944 (1990).

[13] J. W. Cooper and E. B. Saloman, Phys. Rev. A **26**, 1452 (1982).

[14] C. T. W. Lahaye and W. Hogervorst, Phys. Rev. A **39**, 5658 (1989).

[15] R. D. Knight and L.-G. Wang, Phys. Rev. A **32**, 896 (1985).

[16] P. F. Brevet, M. Pellarin, and J. L. Vialle, Phys. Rev. A **42**, 1460 (1990).

[17] H. J. Silverstone, Phys. Rev. A **18**, 1853 (1978); H. J. Silverstone, B. G. Adams, J. Cizek, and P. Otto, Phys.

Rev. Lett. **43**, 1498 (1979).
[18] E. Luc-Koenig and L. Bachelier, J. Phys. B **13**, 1743 (1980); **13**, 1769 (1980).
[19] R. J. Damburg and V. V. Kolosov, J. Phys. B **9**, 3149 (1976); Phys. Lett. **61A**, 233 (1977); J. Phys. B **11**, 1921 (1978); **12**, 2637 (1979); R. J. Damburg and V. V. Kolosov, in *Rydberg States of Atoms and Molecules,* edited by R. F. Stebbings and F. B. Dunning (Cambridge University Press, Cambridge, England, 1983).
[20] U. Fano, Phys. Rev. A **24**, 619 (1981).
[21] D. A. Harmin, Phys. Rev. A **24**, 2491 (1981); **26**, 2656 (1982); **30**, 2413 (1984).
[22] D. A. Harmin, Comments At. Mol. Phys. **15**, 281 (1985).
[23] K. Sakimoto, J. Phys. B **19**, 3011 (1986); **22**, 2727 (1989).
[24] G. Jalbert, P. Labastie, P. F. Brevet, C. Bordas, and M. Broyer, Phys. Rev. A **40**, 784 (1989).
[25] P. F. Brevet, C. Bordas, M. Broyer, G. Jalbert, and P. Labastie, J. Phys. (Paris) **II 1**, 875 (1991).
[26] W. L. Glab and J. P. Hessler, Phys. Rev. Lett. **62**, 1472 (1989); Phys. Rev. A **42**, 5486 (1990).
[27] C. Bordas, P. F. Brevet, M. Broyer, J. Chevaleyre, and P. Labastie, Europhys. Lett. **3**, 789 (1987).
[28] C. R. Mahon, G. R. Janik, and T. F. Gallagher, Phys. Rev. A **41**, 3746 (1990).
[29] C. Bordas and H. Helm (unpublished).
[30] M. Seaver, W. A. Chupka, S. D. Colson, and D. Gauyacq, J. Phys. Chem. **87**, 2226 (1983).
[31] J. W. Cooper, E. B. Saloman, B. E. Cole, and Shardanand, Phys. Rev. A **28**, 1832 (1983).
[32] J. Chevaleyre, C. Bordas, M. Broyer, and P. Labastie, Phys. Rev. Lett. **57**, 3027 (1986); C. Bordas, M. Broyer, J. Chevaleyre, and P. Labastie, J. Phys. (Paris) C7-647 (1987).
[33] H. F. King and K. Morokuma, J. Chem. Phys. **71**, 3213 (1979).
[34] J. K. G. Watson, S. C. Foster, A. R. W. McKellar, P. Bernath, T. Amano, F. S. Pan, M. W. Crofton, R. S. Altman, and T. Oka, Can. J. Phys. **62**, 1875 (1984).
[35] G. Herzberg and Ch. Jungen, J. Mol. Spectrosc. **41**, 425 (1972).
[36] M. Lombardi, P. Labastie, C. Bordas, and M. Broyer, J. Chem. Phys. **89**, 3479 (1988).
[37] C. Bordas, L. J. Lembo, and H. Helm, Phys. Rev. A **44**, 1817 (1991).
[38] H. Helm, Phys. Rev. Lett. **56**, 42 (1986).
[39] H. Helm, Phys. Rev. A **38**, 3425 (1988).
[40] L. J. Lembo, C. Bordas, and H. Helm, Phys. Rev. A **42**, 6660 (1990).
[41] L. J. Lembo, H. Helm, and D. L. Huestis, J. Chem. Phys. **90**, 5299 (1989).
[42] A. Dohdy, W. Ketterle, H.-P. Messmer, and H. Walther, Chem. Phys. Lett. **151**, 133 (1988); W. Ketterle, H.-P. Messmer, and H. Walther, Europhys. Lett. **8**, 333 (1989).
[43] N. Bjerre, I. Hazell, and D. C. Lorents (unpublished).
[44] C. Bordas and H. Helm, Phys. Rev. A **43**, 3645 (1991).
[45] One atomic unit of electric field is $5.142\,28\times10^{9}$ V/cm; one atomic unit of energy is 219 474.63 cm^{-1}.
[46] G. I. Gellene and R. F. Porter, J. Chem. Phys. **79**, 5975 (1983).
[47] C. Bordas, P. C. Cosby, and H. Helm, J. Chem. Phys. **93**, 6303 (1990).
[48] I. Dabrowski and G. Herzberg, Can. J. Phys. **58**, 1238 (1980).
[49] T. Amano, J. Chem. Phys. **92**, 6492 (1990).
[50] N. G. Adams, D. Smith, and E. Alge, J. Chem. Phys. **81**, 1778 (1984).
[51] H. Hus, F. Youssif, A. Sen, and J. B. A. Mitchell, Phys. Rev. A **38**, 658 (1988).
[52] M. Jungen, J. Chem. Phys. **71**, 3540 (1979).
[53] R. L. Martin, J. Chem. Phys. **71**, 3541 (1979).
[54] A. R. Edmonds, *Angular Momentum in Quantum Mechanics* (Princeton University Press, Princeton, 1957).
[55] A. R. Edmonds, J. Picart, N. Tran. Minh, and R. Pullen, J. Phys. B **12**, 2781 (1979).
[56] J. Tennyson, O. Brass, and E. Pollak, J. Chem. Phys. **92**, 3005 (1990).
[57] Ch. Nager and M. Jungen, Chem. Phys. **70**, 189 (1982).

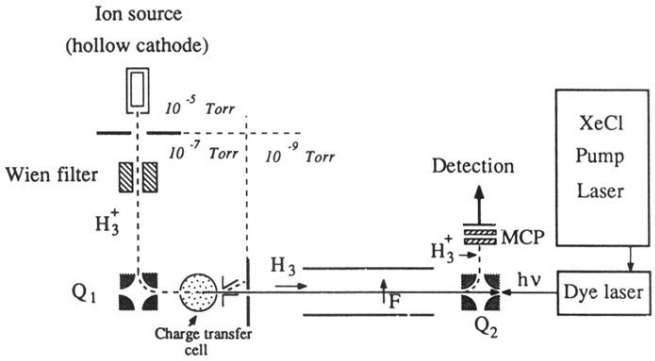

FIG. 1. Experimental setup. The H_3^+ ions produced in a hollow-cathode discharge are mass selected in a Wien filter, deflected in the electrostatic quadrupole Q_1, and then neutralized in the cesium charge-transfer cell. The resulting fast H_3 beam is collinearly excited by the pulsed laser beam. The neutral molecules that are excited but not ionized in the Stark field are field ionized in Q_2, and the H_3^+ ions are detected on a tandem microchannel plate (MCP) and counted during an appropriate time gate.